

1 Favorable Conditions for Magnetic Reconnection at Ganymede's Upstream Magnetopause

2

3 N. Kaweeyanun¹, A. Masters¹, X. Jia²

4

5 ¹Department of Physics, Imperial College London, Prince Consort Road, London, UK.

6 ²Department of Climate and Space Sciences and Engineering, University of Michigan, Ann
7 Arbor, Michigan, USA.

8

9 Corresponding author: N. Kaweeyanun

10 Corresponding author email: nk2814@ic.ac.uk

11

12 **Key Points**

- 13 • We create the first analytical model of conditions at Ganymede-Jupiter magnetopause
14 and assess magnetic reconnection onset theory.
- 15 • Reconnection may occur anywhere on the magnetopause where Ganymede's closed
16 magnetic field meets the ambient field of Jupiter.
- 17 • The average reconnection rate at Ganymede exhibits a Jovian-diurnal variation and
18 hence is driven by Jupiter's rotation.

19 **Abstract**

20 Ganymede is the only Solar System moon known to generate a permanent magnetic field.
21 Jovian plasma motions around Ganymede create an upstream magnetopause, where energy
22 flows are thought to be driven by magnetic reconnection. Simulations indicate Ganymedean
23 reconnection events may be transient, but the nature of magnetopause reconnection at
24 Ganymede remains poorly understood, requiring an assessment of reconnection onset theory.
25 We present an analytical model of steady-state conditions at Ganymede's magnetopause, from
26 which the first Ganymedean reconnection onset assessment is conducted. We find that
27 reconnection may occur wherever Ganymede's closed magnetic field encounters Jupiter's
28 ambient magnetic field, regardless of variations in magnetopause conditions. Unrestricted
29 reconnection onset highlights possibilities for multiple X-lines or widespread transient
30 reconnection at Ganymede. The reconnection rate is controlled by the ambient Jovian field
31 orientation and hence driven by Jupiter's rotation. Future progress on this topic is highly
32 relevant for the JUper ICy moon Explorer (JUICE) mission.

33

34 **Plain Language Summary**

35 Ganymede is the largest moon of Jupiter and the only Solar System moon that produces its own
36 magnetic field. Ganymede's magnetic field is surrounded by Jupiter's much larger magnetic
37 field, which flows around the moon like a river flowing around a rock. The boundary where
38 Jupiter's magnetic field first encounters Ganymede's is called the magnetopause. At this
39 boundary, energy and mass can move between the two magnetic fields through a process called
40 magnetic reconnection. Our paper introduces a simple model of Ganymede's magnetopause,
41 and uses this model to show where reconnection can occur on the boundary. We find that
42 reconnection can occur anywhere on the magnetopause for any plausible environmental

43 conditions around Ganymede, so the locations where these energy-releasing events occur may
44 be particularly unpredictable. The rate of energy released by reconnection meanwhile depends
45 on near-Ganymede conditions, which change significantly as Jupiter rotates. These results will
46 help inform the planning of the JUperiter ICy moon Explorer (JUICE) mission to Ganymede.

47

48 **Keywords**

49 Ganymede, magnetic reconnection, magnetopause, modeling

50

51 **1. Introduction**

52 Ganymede (radius $R_G = 2,634$ km) is the largest moon of Jupiter (equatorial radius $R_J = 71,492$
53 km) and the Solar System. Ganymede uniquely generates a permanent magnetic field as
54 discovered by measurements from both the magnetometer (Kivelson et al., 1997; Kivelson et
55 al., 1996) and the plasma wave subsystem aboard the Galileo spacecraft (Gurnett et al., 1996).
56 The permanent magnetic field is likely dipolar and produced by dynamo action within
57 Ganymede's molten iron core (Anderson et al., 1996; Schubert et al., 1996). The equatorial
58 surface dipole strength is 719 nT, ~ 7 times stronger than the ambient Jovian magnetic field,
59 and the dipole axis typically tilts $\sim 176^\circ$ from Ganymede's spin axis (Kivelson et al., 2002).
60 The dipole axis orientation varied over the short time scales between Galileo flybys, thought
61 to be very likely due to an additional, induced magnetic field arising from electromagnetic
62 induction in a subsurface ocean (Kivelson et al., 2002). Obtaining detailed knowledge of this
63 potentially life-sustaining water source is the primary objective for the upcoming JUperiter ICy
64 moon Explorer (JUICE) mission (Grasset et al., 2013).

65

66 Ganymede orbits Jupiter at an average distance of $\sim 15 R_J$ in a plane nearly coplanar to Jupiter's
67 spin equator (Bills, 2005; McKinnon, 1997). The orbital plane is $\sim 7^\circ$ inclined with respect to
68 the central plane of a $\sim 3 R_J$ thick, rotating Jovian magnetospheric plasma sheet arising from
69 Io's volcanic activity (Kivelson et al., 2004). Ganymede thus effectively moves up and down
70 through the plasma sheet experiencing large variations in the ambient plasma and magnetic
71 conditions. Inside the plasma sheet, there also exists a thin current sheet approximately
72 coplanar to the plasma sheet's central plane (e.g. Cowley et al., 2003). Hence, the ambient
73 Jovian magnetized plasma conditions at Ganymede are controlled by the distance between
74 Ganymede and the center of Jupiter's current sheet.

75

76 The Jovian plasma rotates with the planet at $\sim 80\%$ of the corotation speed at Ganymede
77 (Williams, Mauk, McEntire, 1997; Williams, Mauk, McEntire, Roelof, et al., 1997), which is
78 much faster than Ganymede's Keplerian speed. Hence, the magnetic field frozen into the
79 plasma compresses Ganymede's magnetic field on the upstream side forming a magnetopause
80 boundary (Jia et al., 2008). The Jovian plasma flow is sub-Alfvénic so the magnetic pressure
81 predominantly shapes magnetopause interactions (Neubauer, 1998). Consequently,
82 Ganymede's magnetosphere is cylindrically-shaped with long Alfvén wings and no bow shock
83 preceding the magnetopause (Jia, Kivelson, et al., 2010) - a contrast to planetary
84 magnetospheres which are bullet-shaped due to dynamic pressure dominance in the super-
85 Alfvénic solar wind (Neubauer, 1990). Magnetic field lines near the upstream equator inside
86 the magnetosphere are closed (both ends at Ganymede's magnetic poles) and almost
87 antiparallel (due to 176° dipole tilt) to Jupiter's magnetic field lines, which hints at magnetic
88 reconnection as the dominant mechanism for plasma and energy inflows from Jupiter to
89 Ganymede. Elsewhere, magnetic field lines in Ganymede's large polar caps and magnetotail
90 are open (at least one end at Jupiter), allowing particles entries/escapes from the moon's

91 magnetosphere (Frank et al., 1997; Williams, Mauk, McEntrie, 1997; Williams, Mauk,
92 McEntrie, Roelof, et al., 1997).

93

94 The Ganymede magnetosphere has been modeled by many numerical simulations, some of
95 which discuss magnetic reconnection at the upstream magnetopause. For instance, Jia et al.
96 (2008; 2009) produced a global three-dimensional resistive magnetohydrodynamic (MHD)
97 simulation of Ganymede that showed transient reconnection signatures spread over large
98 regions of the magnetopause. Subsequent analysis revealed these signals to be consistent with
99 intermittent rope-like flux-transfer events (Jia, Walker, et al., 2010). Recently, modeling work
100 has been extended to include the Hall effect (Dorelli et al., 2015), and to couple with kinetic-
101 ion hybrid (Leclercq et al., 2016) and local particle-in-cell codes (Daldorff et al., 2014; Tóth et
102 al., 2016; Zhou et al., 2019), all of which treat reconnection microphysics more directly.
103 Specifically, the MHD-EPIC (embedded particle-in-cell) model indicated presence of
104 quasiperiodic formation of flux-transfer events consistent with previous resistive-MHD results
105 and Galileo observations. However, these comprehensive numerical modelling studies have
106 not been supported by important assessment of reconnection at Ganymede's magnetopause that
107 apply reconnection onset theory, which is an essential additional element in understanding the
108 physics at work.

109

110 We have used an analytical approach to parametrize the magnetopause conditions expected
111 from a typical Jovian plasma flow around Ganymede. This approach provides a
112 computationally cheap way to apply modern kinetic physics of reconnection onset that is
113 challenging to implement in more expensive numerical models. Reconnection onset has been
114 analytically assessed at Earth (Alexeev et al., 1998; Trattner et al., 2007a, 2007b), Jupiter

115 (Desroche et al., 2012; Masters, 2017), Saturn (Desroche et al., 2013; Masters, 2015a), Uranus
 116 (Masters, 2014), and Neptune (Masters, 2015b). In the following sections, we outline the
 117 analytical model of Ganymede's upstream magnetopause followed by the first kinetic
 118 assessment of magnetic reconnection onset and structural properties.

119

120 **2. Analytical Model of Ganymede's Upstream Magnetopause**

121 Maps of conditions immediately either side of Ganymede's magnetopause are essential for
 122 reconnection onset assessment. To achieve this, we must first define the magnetopause surface.
 123 Kivelson et al. (1998) describe Ganymede's magnetosphere as a cylinder with shifting center
 124 points in dynamical Ganymede-at-origin Jovian magnetic field-aligned coordinates (GphiB).
 125 We rewrite the equations for Ganymede's magnetopause surface in Ganymede-at-origin
 126 Cartesian coordinates (GphiO) in which X points along the plasma flow direction, Y points
 127 from Ganymede to Jupiter, and Z points along Jupiter's spin axis (approximately parallel to
 128 Ganymede's spin axis due to small Ganymede orbit inclination) as follows

$$129 \quad f(X, Y, Z) = \frac{(X - X_0)^2}{a^2} + \frac{(Y \cos \theta_r - Z \sin \theta_r - Y_0)^2}{b^2} = 1$$

130 where

$$131 \quad \theta_r = \tan^{-1} \left(\frac{|B_{0,z}|}{B_{0,y}} \right) - 90^\circ$$

$$132 \quad X_0(Y, Z) = X_0(0) + |Y \sin \theta_r + Z \cos \theta_r| \tan \theta$$

$$133 \quad Y_0(Y, Z) = \frac{2}{\pi} Y_{0,max} \sin(\phi - 248^\circ) \tan^{-1} \left(\frac{Y \sin \theta_r + Z \cos \theta_r}{\lambda} \right)$$

134 The angle θ_r describes right-handed rotation angle between GphiB and GphiO coordinates.
 135 $(B_{0,y}, B_{0,z})$ are the ambient Jovian magnetic field components. (X_0, Y_0) denote the center point

136 offsets from the GphiO origin. Kivelson et al. (1998) chose $a = 2.2 R_G$ and $\lambda = 0.5 R_G$, and
137 then used a least squares fit to the Galileo data to calculate $b = 2.90 R_G$, $X_0(0) = 0.544 R_G$,
138 $Y_{0,max} = 0.914 R_G$, and $\theta = 0.298$ radians. This leaves Jupiter's System-III east longitude ϕ
139 as the only free parameter. System-III coordinates describe a stationary Jovian magnetic dipole
140 with Ganymede orbiting quickly through the longitudes, which is equivalent to a rapidly
141 spinning dipole in Ganymede-stationary GphiO coordinates. As the Jovian plasma/current
142 sheets move with the dipole, each ϕ value determines their positions relative to Ganymede, and
143 thus ambient plasma/magnetic conditions that control reconnection.

144

145 From these equations we can generate Ganymede's upstream ($X < 0 R_G$) magnetopause grid
146 surface between $-4.0 R_G < Y < 4.0 R_G$ and $-1.0 R_G < Z < 1.0 R_G$ with $0.01 R_G$ resolution
147 in both dimensions. The magnetopause is projected onto a Y-Z plane as shown in Figure 1A
148 when Ganymede is in the Jovian current sheet ($\phi = 248^\circ$). Here the magnetopause is north-
149 south symmetric with the standoff distance of $1.65 R_G$ calculated at the subflow point ($Y = 0$
150 R_G , $Z = 0 R_G$). The magnetopause X-coordinate increases away from the subflow point in all
151 directions as the surface curves downstream. The magnetopause gains maximum north-south
152 asymmetries when Ganymede is furthest above/below the current sheet ($\phi = 158^\circ, 338^\circ$).
153 These asymmetries occur in response to changes in ambient Jovian magnetic field orientations
154 (parametrization below). This simple and fixed magnetopause description is sufficient for
155 reconnection onset assessment, as more accurate surface models will not affect the conclusions
156 drawn.

157

158 Next, we describe the Jovian-side (external) conditions at the magnetopause. The ambient
159 Jovian plasma mass density is $\rho_0 = 56 \text{ amu/cm}^3$ when Ganymede is in the current sheet and

160 $\rho_0 = 28 \text{ amu/cm}^3$ when Ganymede is furthest above/below the current sheet (Jia et al., 2008).
161 The plasma is compressed near Ganymede's magnetopause thus increasing its mass density.
162 We employ a simple compression formula $\rho_J = A_1 \cos(\alpha) + \rho_0$ where α is the flaring angle
163 between the X-axis and the local magnetopause-normal vector. The cosine of flaring angle is
164 adapted from results at Earth's magnetopause (Petrinec & Russell, 1997) and captures spatial
165 density variations expected from plasma flows around a cylindrical magnetosphere. A more
166 complex compression description is again possible but unlikely to affect main conclusions
167 drawn. The typical compression amplitude $A_1 = 4 \text{ amu/cm}^3$ is estimated empirically from
168 numerical simulations (Jia et al., 2008; Tóth et al., 2016) and the added ambient mass density
169 ρ_0 prevents plasma decompression. Figure 1B shows the Jovian-side mass density variation
170 when Ganymede is in the current sheet. The density peaks near the subflow point where Jovian
171 plasma collides head-on with the magnetopause and decreases toward the flanks where plasma
172 flows near-parallel to the surface.

173

174 The ambient Jovian plasma pressure (thermal and energetic) is $P_0 = 3.8 \text{ nPa}$ when Ganymede
175 is in the current sheet and $P_0 = 1.9 \text{ nPa}$ when Ganymede is furthest above/below the current
176 sheet (Jia et al., 2008; Kivelson et al., 2004). Figure 1C shows plasma pressure at the Jovian-
177 side magnetopause when Ganymede is in the current sheet. Like mass density, a cosine relation
178 $P_{J,p} = A_2 \cos(\alpha) + P_0$ parametrizes the pressure compression. The amplitude $A_2 = 1.05 \text{ nPa}$ is
179 approximated from the pressure relation at Earth's magnetopause for slow plasma flow speeds
180 (Petrinec & Russell, 1997). This method provides slightly smaller Jovian-side plasma pressures
181 ($\sim 1 \text{ nPa}$ difference) compared to numerically simulated values. However, larger pressures are
182 found to cause unrealistic Jovian magnetic field decompression at the magnetopause (discussed
183 below).

184

185 The ambient Jovian plasma flows along the X-axis at speed $v_0 = 140$ km/s in Ganymede's rest
186 frame (Jia et al., 2008). Figure 1D shows the plasma flow velocity at the Jovian-side
187 magnetopause when Ganymede is in the current sheet. Unlike mass density and pressure, we
188 parametrize the flow speed by a sine relation $v_J = v_0 \sin(\alpha)$ as the ambient plasma is most
189 stagnated by direct collision near the subflow point. The Jovian-side flow directions
190 (normalized arrows) are constrained to be parallel to the magnetopause surface and orthogonal
191 to cross products of magnetopause-normal vectors and ambient plasma flow vectors.

192

193 The ambient Jovian magnetic field has been computed at Ganymede using a mathematical
194 model (Jia et al., 2008; Khurana, 1997). The magnetic field strength has minima of $B_0 \sim 70$
195 nT when Ganymede is in the current sheet and maxima of $B_0 \sim 105$ nT when Ganymede is
196 furthest above/below the current sheet. Following Jia et al. (2008), we assume negligible x-
197 component $B_{0,x}$ and parametrize the remaining two components by $B_{0,y} = 84 \sin(\phi - 248^\circ)$
198 nT and $B_{0,z} = 3 \cos(\phi) - 79$ nT. Hence, the ambient Jovian magnetic field always points
199 southward in the Y-Z plane between 135° - 225° clock angles. We quantify magnetic field
200 compression at the Jovian-side magnetopause using conservation of combined magnetic,
201 plasma, and dynamic pressures before and after the compression. The total pre-compression
202 pressure can be calculated from ambient plasma/magnetic values. Using data from Figures 1C
203 and 1D, we derive post-compression plasma pressure and magnetopause-parallel dynamic
204 pressure component. We subtract these values from the total pressure to obtain the post-
205 compression magnetic pressure $P_{J,b}$ (which includes the magnetopause-normal dynamic
206 pressure component) and convert this into Jovian-side magnetic field strength B_J shown in

207 Figure 1E when Ganymede is in the current sheet. The plasma compression also constrains
208 magnetic field directions (normalized arrows) onto the magnetopause surface.

209

210 The Jovian-side plasma and magnetic pressures together exert force on Ganymede's
211 magnetopause, which is balanced by magnetic pressure from Ganymede's magnetic field given
212 negligible plasma pressure inside the moon's magnetosphere (Jia et al., 2008). Hence, we can
213 derive the magnetic field strength at the Ganymede-side magnetopause B_G as shown in
214 Figure 1F when Ganymede is in the current sheet. Magnetic field directions (normalized
215 arrows) have no azimuthal component (consistent with dipolar field) and lie parallel to the
216 magnetopause surface. The magnetic field points northward in the "closed-field region"
217 defined by $|Z| < 0.63 R_G$ and southward elsewhere (Jia et al. 2009). The closed-field region
218 is bounded by two horizontal red dashed lines which we retroactively add to all Figure 1
219 subplots. Otherwise, the Ganymede-side plasma density and flow speed are set to uniform
220 values $\rho_G = 20 \text{ amu/cm}^3$ (Jia et al. 2008, 2009) and $v_G = 0 \text{ km/s}$ (approximating relatively
221 slow plasma flows inside Ganymede's magnetosphere) respectively.

222

223 **3. Magnetic Reconnection Assessment at Ganymede**

224 With maps of conditions on both sides of Ganymede's magnetopause, we can assess
225 reconnection onset specifically for the closed-field region where particle transport is not
226 expected under MHD theory. Reconnection onset requires three conditions to be satisfied. First,
227 the magnetopause current sheet separating Jupiter's and Ganymede's magnetic fields must be
228 thinner than approximately an ion inertial length to break the MHD frozen-in flux condition
229 (Phan et al., 2011). The Galileo data analysis revealed the magnetopause current sheet
230 thickness to be $< 400 \text{ km}$ (Kivelson et al., 1998), similar to the $\sim 426 \text{ km}$ ion inertial length

231 calculated from magnetopause conditions in Figure 1. Hence, we can assume a sufficiently thin
232 magnetopause current sheet irrespective of Ganymede's position relative to the Jovian current
233 sheet.

234

235 The remaining two onset conditions effectively limit local plasma flows to be below the
236 characteristic Alfvén speed associated with reconnection, with suppression of reconnection
237 above this limit. The second onset condition concerns the diamagnetic drift between plasma
238 electrons and ions within the magnetopause current sheet, leading to a condition involving the
239 magnetic shear angle

$$240 \quad \theta_{\text{sh}} > 2 \tan^{-1} \left(\frac{d_i \Delta\beta}{L} \right) = 2 \tan^{-1}(\Delta\beta)$$

241 where θ_{sh} is the smaller shear angle between the Jovian and Ganymedean magnetic fields in a
242 magnetopause-tangent plane at each grid point (Swisdak et al., 2003; 2010). If this condition
243 is unsatisfied, the diamagnetic drift is too fast and reconnection is suppressed. The system
244 length scale (L) is the magnetopause current sheet thickness, which from the first onset
245 condition is approximately equal to the ion inertial length (d_i), so the shear angle minimum
246 threshold depends only on the beta difference ($\Delta\beta = \beta_J - \beta_G$) across the magnetopause. As
247 Ganymede contributes negligible plasma pressure ($\beta_G = 0$), $\Delta\beta$ is equal to the Jovian-side beta
248 $\beta_J = P_{J,p}/P_{J,b}$. The third onset condition concerns the flow shear between Jovian and
249 Ganymedean bulk plasmas adjacent to the magnetopause current sheet along the reconnection
250 outflow direction. Each magnetopause location has two outflow vectors parallel/antiparallel to
251 the cross product of the vector bisecting the smaller shear angle between Jovian and
252 Ganymedean magnetic field lines and the local magnetopause-normal vector (Masters, 2017).

253 We choose the southward-pointing primary outflow vector following the Jovian field lines, and
 254 define the flow shear condition

$$255 \quad v_{\text{sh}} = \frac{|v_1 - v_2|}{2} < v_{\text{out}} \left(\frac{\rho_1 B_2 + \rho_2 B_1}{2(\rho_1 B_2 \rho_2 B_1)^{1/2}} \right)$$

$$256 \quad v_{\text{out}} = \left(\frac{B_1 B_2 (B_1 + B_2)}{\mu_0 (\rho_1 B_2 + \rho_2 B_1)} \right)^{1/2}$$

257 where symbol definitions are v = flow velocity, ρ = mass density, B = magnetic field strength,
 258 and $\mu_0 = 4\pi \times 10^{-7}$ H/m (Doss et al., 2015). Subscripts 1 and 2 indicate parameter projections
 259 along the outflow vector on Jovian-side and Ganymede-side respectively. The flow shear is
 260 $v_{\text{sh}} = |v_1 - v_2|/2$ and the outflow speed is v_{out} . Reconnection is suppressed if the flow shear
 261 exceeds its maximum threshold.

262

263 We first assess these two onset conditions for a specific case when Ganymede is in the Jovian
 264 current sheet, and then consider two extreme cases when Ganymede is furthest above/below
 265 the current sheet. Figure 2 assesses the diamagnetic drift condition when Ganymede is in the
 266 current sheet. Beta differences in Figure 2A have the average of 2.02 in the closed-field region,
 267 with largest $\Delta\beta$ along the magnetopause flanks where the Jovian-side magnetic field is weakest.
 268 The resulting shear angle minimum thresholds ($\theta_{\text{sh,min}}$) in Figure 2B have the average of 90.3°
 269 with largest values along the flanks. Figure 2C shows magnetic shear angles calculated using
 270 data from Figures 1E and 1F. The average θ_{sh} is 175° with largest values in columns nearest
 271 to the subflow point and toward the flanks. Comparing Figures 2B and 2C indicates that $\theta_{\text{sh}} >$
 272 $\theta_{\text{sh,min}}$ at every point in the closed-field region, satisfying the second onset condition
 273 everywhere on Ganymede's magnetopause.

274

275 Figure 3 assesses the flow shear condition when Ganymede is in the current sheet.
276 Reconnection outflow speeds in Figure 3A have the average of 327 km/s in the closed-field
277 region with largest values along columns near the subflow point, where magnetic fields are
278 most strongly aligned with outflow vectors. The resulting maximum flow shear thresholds
279 ($v_{sh,max}$) in Figure 3B have the average of 443 km/s with largest values near the subflow point.
280 Figure 3C shows flow shears calculated from the Jovian plasma flow in Figure 1D. The average
281 v_{sh} is 13.7 km/s with largest values near the subflow point from outflow-aligned magnetic
282 fields. Flow shears are also noticeably smaller along $Z = 0$ line where the Jovian plasma flow
283 stagnates. Comparing Figures 3B and 3C indicates that $v_{sh} < v_{sh,max}$ at every point in the
284 closed-field region, satisfying the third onset condition everywhere on Ganymede's
285 magnetopause.

286

287 Consequently, magnetic reconnection can occur anywhere on Ganymede's magnetopause
288 when Ganymede is in the current sheet. The electric field associated with reconnection follows
289 (Doss et al., 2015)

290

$$E = 2k \left(\frac{B_1 B_2}{B_1 + B_2} \right) v_{out} \left(1 - \frac{(v_1 - v_2)^2}{(v_{out})^2} \frac{\rho_1 B_2 \rho_2 B_1}{(\rho_1 B_2 + \rho_2 B_1)^2} \right)$$

291 where the near-Earth reconnection efficiency factor $k = 0.1$ is adopted as it has no known β -
292 dependence (e.g. Paschmann et al., 2013, Masters 2017). Figure 4A shows the electric field
293 when Ganymede is in the current sheet with average magnitude 3.2 mV/m. Strongest field
294 magnitudes are found along near-subflow columns corresponding to largest outflow speed
295 locations. We also track (following Cooling et al., 2001) parcels of plasma in reconnection
296 outflows from three equatorial reconnection sites – one at the subflow point and two others at

297 mid-flanks ($Y = \pm 1.5 R_G$). All outflows travel bidirectionally north/south away from
298 Ganymede's equator. However, the subflow site's outflows remain on the magnetopause
299 symmetry plane ($Z = 0$) while the mid-flank sites' outflows shift toward their nearest flanks
300 due to influence from the Jovian-side plasma flow.

301

302 Figures 4B and 4C respectively show reconnection assessment when Ganymede is furthest
303 above and below the current sheet, with magnetopause asymmetries and ambient parameters
304 adjusted accordingly. Despite condition changes, the electric fields remain non-zero throughout
305 closed-field regions, so reconnection is also possible anywhere on the magnetopause when
306 Ganymede is furthest above/below the current sheet. The electric field varies symmetrically
307 north/south of the current sheet and becomes stronger along the flanks where Jupiter's and
308 Ganymede's magnetic fields are now most strongly antiparallel. The average electric field also
309 increases from 3.2 mV/m to 5.1 mV/m at extreme Ganymede positions. Small discontinuities
310 are observed across lines containing the subflow point, reflecting sharp turns on the
311 magnetopause arising from the surface equations. A more realistic magnetopause surface
312 would be smoother, and so the discontinuities should disappear.

313

314 **4. Discussion**

315 Since there appears to be no restrictions for reconnection onset when Ganymede's
316 magnetopause is symmetric and most asymmetric, we can generalize that reconnection is
317 favorable anywhere on the magnetopause for all magnetopause asymmetries i.e. all positions
318 along Ganymede's orbit of Jupiter. This result is consistent with widespread reconnection
319 events observed in global simulations (e.g. Jia, Walker, et al., 2010; Tóth et al., 2016)

320

321 The electric field magnitude range (2.6 – 5.6 mV/m) modelled is much larger compared to
322 those at Earth's (<0.01 – 0.2 mV/m) and Jupiter's (<0.1 mV/m) magnetopauses (Paschmann et
323 al., 2013; Masters, 2017), indicating significant reconnection rates at all Ganymedean
324 magnetopause locations. Although a dominant X-line is possible, this electric field
325 configuration highlights possibilities for less ordered reconnection site distributions, such as
326 multiple large X-lines or widespread transient flux-transfer events (seen in global simulations),
327 at Ganymede's magnetopause.

328

329 The electric field equation is found most sensitive to changes in magnetic parameters B_1 and
330 B_2 . As Ganymede moves further away from the Jovian current sheet, the ambient Jovian
331 magnetic field becomes stronger, increasing both B_1 and B_2 (the latter due to the model's fixed
332 magnetopause surface). The average electric field increases in Figure 4 are therefore dependent
333 on Ganymede's position and controlled by Jupiter's east longitude ϕ . As the Jovian dipole
334 rotates rapidly, each ϕ value also corresponds to a distinct time-of-day on Jupiter. Hence
335 magnetic reconnection rate at Ganymede exhibits a Jovian-diurnal variation and is effectively
336 driven by Jupiter's rotation. The conclusion has been independently supported by remote
337 observations of Jovian radio emissions associated with Ganymede (Zarka et al., 2018).

338

339 Multiplying the average electric fields by the magnetopause width ($\sim 6 R_G$) gives 50-80 kV
340 reconnection voltage estimates at Ganymede's magnetopause, which may be used to constrain
341 reconnection rate in the magnetotail via open magnetic flux conservation. We also calculate
342 reconnection-induced electron and ion temperature increases of 250-560 eV and 2,000-4,200
343 eV respectively using empirical methods from Earth-based studies (Phan et al., 2013; 2014),
344 with the maximum (minimum) value corresponding to when Ganymede is furthest

345 above/below (in) the Jovian current sheet. These numbers far exceed ambient temperatures for
346 electrons and ions of 300 eV and 60 eV respectively (Kivelson et al., 2004), hence reconnection
347 should result in particle heating signatures observable by the upcoming JUICE mission.

348

349 **5. Summary**

350 Ganymede's permanent magnetic field and its resulting magnetosphere present a unique
351 opportunity to study magnetic reconnection in a sub-Alfvénic plasma flow environment. We
352 present an analytical model of steady-state conditions at Ganymede's upstream magnetopause,
353 from which we conduct the first assessment of reconnection onset theory at this boundary. The
354 model shows that reconnection may occur anywhere on the magnetopause where Ganymede's
355 closed magnetic field encounters Jupiter's ambient field, and the onset appears largely
356 unaffected by Ganymede's position relative to the Jovian current sheet. This result is consistent
357 with previous global MHD simulations of Ganymede's magnetosphere, and highlights
358 possibilities for less orderly reconnection structures (multiple X-lines, widespread flux-transfer
359 events) at Ganymede's magnetopause.

360

361 The average reconnection rate is shown to be a function of Ganymede's position along its orbit
362 around Jupiter, which approximately corresponds to the time-of-day on Jupiter. Hence, the
363 reconnection rate exhibits a Jovian-diurnal variation and is effectively driven by Jupiter's
364 rotation. The reconnection process should heat up surrounding plasma particles producing
365 signatures detectable by spacecraft instruments. Our steady-state model currently does not
366 capture orientation changes of Ganymede's magnetic field due to the moon's subsurface ocean.
367 Future integration of ocean effects will allow more accurate predictions of reconnection
368 structures in preparation for the JUICE space mission.

370 Acknowledgements

371 NK is supported by a Royal Society PhD Studentship, and AM is supported by a Royal Society
372 University Research Fellowship. Derived data in Figures 1-4 is available in the Imperial
373 College High Performance Computing Service Data Repository (doi:10.14469/hpc/6738).

374 **Reference**

- 375 Alexeev, I. I., Sibeck, D. G., & Bobrovnikov, S. Y. (1998). Concerning the location of
376 magnetopause merging as a function of the magnetopause current strength. *Journal of*
377 *Geophysical Research: Space Physics*, 103(A4), 6675--6684. doi:10.1029/97JA02863
- 378 Anderson, J. D., Lau, E. L., Sjogren, W. L., Schubert, G., & Moore, W. B. (1996). Gravitational
379 constraints on the internal structure of Ganymede. *Nature*, 384(6609), 541--543.
380 doi:10.1038/384541a0
- 381 Bills, B. G. (2005). Free and forced obliquities of the Galilean satellites of Jupiter. *Icarus*,
382 175(1), 233--247. doi:10.1016/j.icarus.2004.10.028
- 383 Cooling, B. M. A., Owen, C. J., & Schwartz, S. J. (2001). Role of the magnetosheath flow in
384 determining the motion of open flux tubes. *Journal of Geophysical Research: Space*
385 *Physics*, 106(A9), 18763--18775. doi:10.1029/2000JA000455
- 386 Cowley, S. W. H., Bunce, E. J., & Nichols, J. D. (2003). Origins of Jupiter's main oval auroral
387 emissions. *Journal of Geophysical Research: Space Physics*, 108(A4).
388 doi:10.1029/2002ja009329
- 389 Daldorff, L. K. S., Tóth, G., Gombosi, T. I., Lapenta, G., Amaya, J., Markidis, S., & Brackbill,
390 J. U. (2014). Two-way coupling of a global Hall magnetohydrodynamics model with a
391 local implicit particle-in-cell model. *Journal of Computational Physics*, 268, 236--254.
392 doi:10.1016/j.jcp.2014.03.009
- 393 Desroche, M., Bagenal, F., Delamere, P. A., & Erkaev, N. (2012). Conditions at the expanded
394 Jovian magnetopause and implications for the solar wind interaction. *Journal of*
395 *Geophysical Research: Space Physics*, 117(A7). doi:10.1029/2012JA017621
- 396 Desroche, M., Bagenal, F., Delamere, P. A., & Erkaev, N. (2013). Conditions at the
397 magnetopause of Saturn and implications for the solar wind interaction. *Journal of*
398 *Geophysical Research: Space Physics*, 118(6), 3087--3095. doi:10.1002/jgra.50294

399 Dorelli, J. C., Gloer, A., Collinson, G., & Tóth, G. (2015). The role of the Hall effect in the
400 global structure and dynamics of planetary magnetospheres: Ganymede as a case study:
401 Hall reconnection at Ganymede. *Journal of Geophysical Research: Space Physics*, *120*.
402 doi:10.1002/2014JA020951

403 Doss, C. E., Komar, C. M., Cassak, P. A., Wilder, F. D., Eriksson, S., & Drake, J. F. (2015).
404 Asymmetric magnetic reconnection with a flow shear and applications to the
405 magnetopause. *Journal of Geophysical Research: Space Physics*, *120*(9), 7748--7763.
406 doi:10.1002/2015JA021489

407 Frank, L. A., Paterson, W. R., Ackerson, K. L., & Bolton, S. J. (1997). Outflow of hydrogen
408 ions from Ganymede. *Geophysical Research Letters*, *24*(17), 2151--2154.
409 doi:10.1029/97GL01744

410 Grasset, O., Dougherty, M. K., Coustenis, A., Bunce, E., Erd, C., Titov, D. V., . . . Van Hoolst,
411 T. (2013). JUPITER ICy moons Explorer (JUICE): An ESA mission to orbit Ganymede
412 and to characterise the Jupiter system. *Planetary and Space Science*, *78*, 1--21.
413 doi:10.1016/j.pss.2012.12.002

414 Gurnett, D. A., Kurth, W. S., Roux, A., Bolton, S. J., & Kennel, C. F. (1996). Evidence for a
415 magnetosphere at Ganymede from plasma-wave observations by the Galileo spacecraft.
416 *Nature*, *384*(6609), 535--537. doi:10.1038/384535a0

417 Jia, X., Kivelson, M. G., Khurana, K. K., & Walker, R. J. (2010). Magnetic Fields of the
418 Satellites of Jupiter and Saturn. *Space Science Reviews*, *152*(1), 271--305.
419 doi:10.1007/s11214-009-9507-8

420 Jia, X., Walker, R. J., Kivelson, M. G., Khurana, K. K., & Linker, J. A. (2008). Three-
421 dimensional MHD simulations of Ganymede's magnetosphere. *Journal of Geophysical*
422 *Research: Space Physics*, *113*(A6). doi:10.1029/2007JA012748

423 Jia, X., Walker, R. J., Kivelson, M. G., Khurana, K. K., & Linker, J. A. (2009). Properties of
424 Ganymede's magnetosphere inferred from improved three-dimensional MHD
425 simulations. *Journal of Geophysical Research: Space Physics*, *114*(A9).
426 doi:10.1029/2009JA014375

427 Jia, X., Walker, R. J., Kivelson, M. G., Khurana, K. K., & Linker, J. A. (2010). Dynamics of
428 Ganymede's magnetopause: Intermittent reconnection under steady external conditions.
429 *Journal of Geophysical Research: Space Physics*, *115*(A12).
430 doi:10.1029/2010JA015771

431 Kaweeyanun, N. (2020). Favorable conditions for magnetic reconnection at Ganymede's
432 upstream magnetopause. Version 1.0. Imperial College High Performance Computing
433 Service Data Repository. <http://dx.doi.org/10.14469/hpc/6738>. Accessed 24 January
434 2020.

435 Khurana, K. K. (1997). Euler potential models of Jupiter's magnetospheric field. *Journal of*
436 *Geophysical Research: Space Physics*, *102*(A6), 11295--11306.
437 doi:10.1029/97JA00563

438 Kivelson, M. G., Bagenal, F., Kurth, W., M. Neubauer, F., Paranicas, C., & Saur, J. (2004).
439 Magnetospheric interactions with satellites. *Jupiter. The Planet, Satellites and*
440 *Magnetosphere*, 513-536.

441 Kivelson, M. G., Khurana, K. K., Coroniti, F. V., Joy, S., Russell, C. T., Walker, R. J., . . .
442 Polansky, C. (1997). The magnetic field and magnetosphere of Ganymede.
443 *Geophysical Research Letters*, *24*(17), 2155--2158. doi:10.1029/97GL02201

444 Kivelson, M. G., Khurana, K. K., Russell, C. T., Walker, R. J., Warnecke, J., Coroniti, F. V., .
445 . . Schubert, G. (1996). Discovery of Ganymede's magnetic field by the Galileo
446 spacecraft. *Nature*, *384*(6609), 537--541. doi:10.1038/384537a0

447 Kivelson, M. G., Khurana, K. K., & Volwerk, M. (2002). The Permanent and Inductive
448 Magnetic Moments of Ganymede. *Icarus*, 157(2), 507--522.
449 doi:<https://doi.org/10.1006/icar.2002.6834>

450 Kivelson, M. G., Warnecke, J., Bennett, L., Joy, S., Khurana, K. K., Linker, J. A., . . .
451 Polansky, C. (1998). Ganymede's magnetosphere: Magnetometer overview. *Journal*
452 *of Geophysical Research: Planets*, 103(E9), 19963--19972. doi:10.1029/98JE00227

453 Leclercq, L., Modolo, R., Leblanc, F., Hess, S., & Mancini, M. (2016). 3D magnetospheric
454 parallel hybrid multi-grid method applied to planet-plasma interactions. *Journal of*
455 *Computational Physics*, 309, 295-313. doi:<https://doi.org/10.1016/j.jcp.2016.01.005>

456 Masters, A. (2014). Magnetic reconnection at Uranus' magnetopause. *Journal of Geophysical*
457 *Research: Space Physics*, 119(7), 5520--5538. doi:10.1002/2014JA020077

458 Masters, A. (2015a). The dayside reconnection voltage applied to Saturn's magnetosphere.
459 *Geophysical Research Letters*, 42(8), 2577--2585. doi:10.1002/2015GL063361

460 Masters, A. (2015b). Magnetic reconnection at Neptune's magnetopause. *Journal of*
461 *Geophysical Research: Space Physics*, 120(1), 479--493. doi:10.1002/2014JA020744

462 Masters, A. (2017). Model-Based Assessments of Magnetic Reconnection and Kelvin-
463 Helmholtz Instability at Jupiter's Magnetopause. *Journal of Geophysical Research:*
464 *Space Physics*, 122(11), 11,154--111,174. doi:10.1002/2017JA024736

465 McKinnon, W. B. (1997). Galileo at Jupiter ---meetings with remarkable moons. *Nature*,
466 390(6655), 23--26. doi:10.1038/36222

467 Neubauer, F. (1998). *The sub-Alfvénic interaction of the Galilean satellites with the Jovian*
468 *magnetosphere* (Vol. 103).

469 Neubauer, F. M. (1990). Satellite plasma interactions. *Advances in Space Research*, 10, 25--
470 38. doi:10.1016/0273-1177(90)90083-C

471 Paschmann, G., Øieroset, M., & Phan, T. (2013). In-Situ Observations of Reconnection in
472 Space. *Space Science Reviews*, 178(2), 385--417. doi:10.1007/s11214-012-9957-2

473 Petrinec, S. M., & Russell, C. T. (1997). Hydrodynamic and MHD equations across the bow
474 shock and along the surface of planetary obstacles. *Space Science Reviews*, 79(3), 757-
475 -791. doi:10.1023/A:1004938724300

476 Phan, T. D., Drake, J. F., Shay, M. A., Gosling, J. T., Paschmann, G., Eastwood, J. P., . . .
477 Angelopoulos, V. (2014). Ion bulk heating in magnetic reconnection exhausts at Earth's
478 magnetopause: Dependence on the inflow Alfvén speed and magnetic shear angle.
479 *Geophysical Research Letters*, 41(20), 7002--7010. doi:10.1002/2014GL061547

480 Phan, T. D., Love, T. E., Gosling, J. T., Paschmann, G., Eastwood, J. P., Oieroset, M., . . .
481 Auster, U. (2011). Triggering of magnetic reconnection in a magnetosheath current
482 sheet due to compression against the magnetopause. *Geophysical Research Letters*,
483 38(17). doi:10.1029/2011GL048586

484 Phan, T. D., Shay, M. A., Gosling, J. T., Fujimoto, M., Drake, J. F., Paschmann, G., . . .
485 Angelopoulos, V. (2013). Electron bulk heating in magnetic reconnection at Earth's
486 magnetopause: Dependence on the inflow Alfvén speed and magnetic shear.
487 *Geophysical Research Letters*, 40(17), 4475--4480. doi:10.1002/grl.50917

488 Schubert, G., Zhang, K., Kivelson, M. G., & Anderson, J. D. (1996). The magnetic field and
489 internal structure of Ganymede. *Nature*, 384(6609), 544--545. doi:10.1038/384544a0

490 Swisdak, M., Opher, M., Drake, J. F., & Alouani Bibi, F. (2010). The vector direction of the
491 Interstellar Magnetic Field Outside the Heliosphere. *710(2)*, 1769-1775.
492 doi:10.1088/0004-637x/710/2/1769

493 Swisdak, M., Rogers, B., F. Drake, J., & Shay, M. (2003). Diamagnetic Suppression of
494 Component Magnetic Reconnection at the Magnetopause. *J. Geophys. Res.*, 108.
495 doi:10.1029/2002JA009726

496 Tóth, G., Jia, X., Markidis, S., Peng, I. B., Chen, Y., Daldorff, L. K. S., . . . Dorelli, J. C. (2016).
497 Extended magnetohydrodynamics with embedded particle-in-cell simulation of
498 Ganymede's magnetosphere. *Journal of Geophysical Research: Space Physics*, *121*(2),
499 1273--1293. doi:10.1002/2015JA021997

500 Trattner, K. J., Mulcock, J. S., Petrinec, S. M., & Fuselier, S. A. (2007a). Location of the
501 reconnection line at the magnetopause during southward IMF conditions. *Geophysical*
502 *Research Letters*, *34*(3). doi:10.1029/2006GL028397

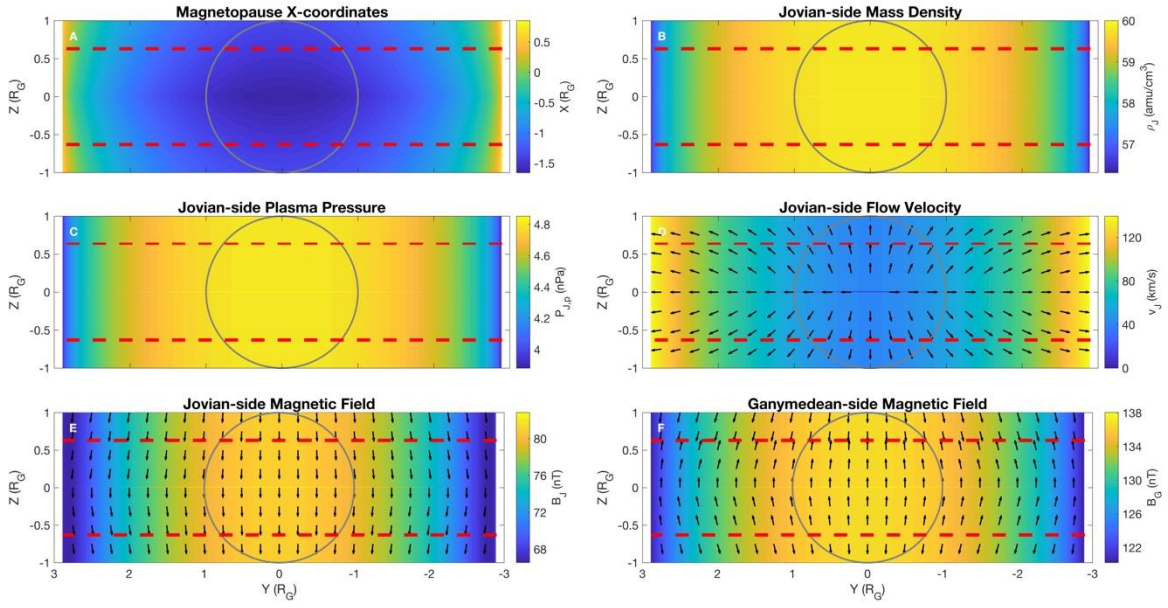
503 Trattner, K. J., Mulcock, J. S., Petrinec, S. M., & Fuselier, S. A. (2007b). Probing the boundary
504 between antiparallel and component reconnection during southward interplanetary
505 magnetic field conditions. *Journal of Geophysical Research: Space Physics*, *112*(A8).
506 doi:10.1029/2007JA012270

507 Williams, D. J., Mauk, B., & McEntire, R. W. (1997). Trapped electrons in Ganymede's
508 magnetic field. *Geophysical Research Letters*, *24*(23), 2953--2956.
509 doi:10.1029/97GL03003

510 Williams, D. J., Mauk, B. H., McEntire, R. W., Roelof, E. C., Armstrong, T. P., Wilken, B., . . .
511 . Murphy, N. (1997). Energetic particle signatures at Ganymede: Implications for
512 Ganymede's magnetic field. *Geophysical Research Letters*, *24*(17), 2163--2166.
513 doi:10.1029/97GL01931

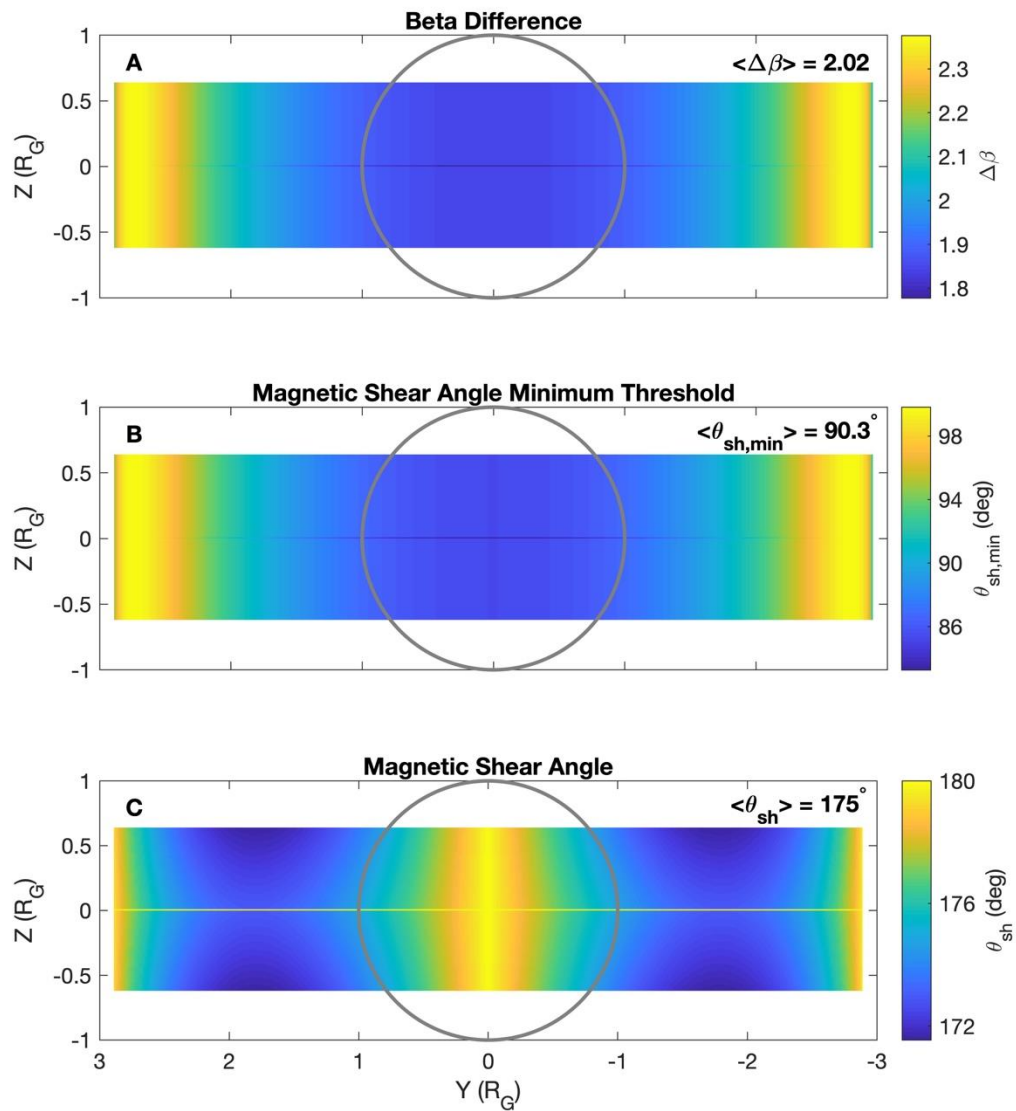
514 Zarka, P., Soares Marques, M., Louis, C., Ryabov, V., Lamy, L., Echer, E., & Cecconi, B.
515 (2018). Jupiter radio emission induced by Ganymede and consequences for the radio
516 detection of exoplanets. *Astronomy & Astrophysics*. doi:10.1051/0004-
517 6361/201833586

518 Zhou, H., Tóth, G., Jia, X., Chen, Y., & Markidis, S. (2019). Embedded Kinetic Simulation
519 of Ganymede's Magnetosphere: Improvements and Inferences. *Journal of Geophysical*
520 *Research: Space Physics*, *0*(0). doi:10.1029/2019JA026643



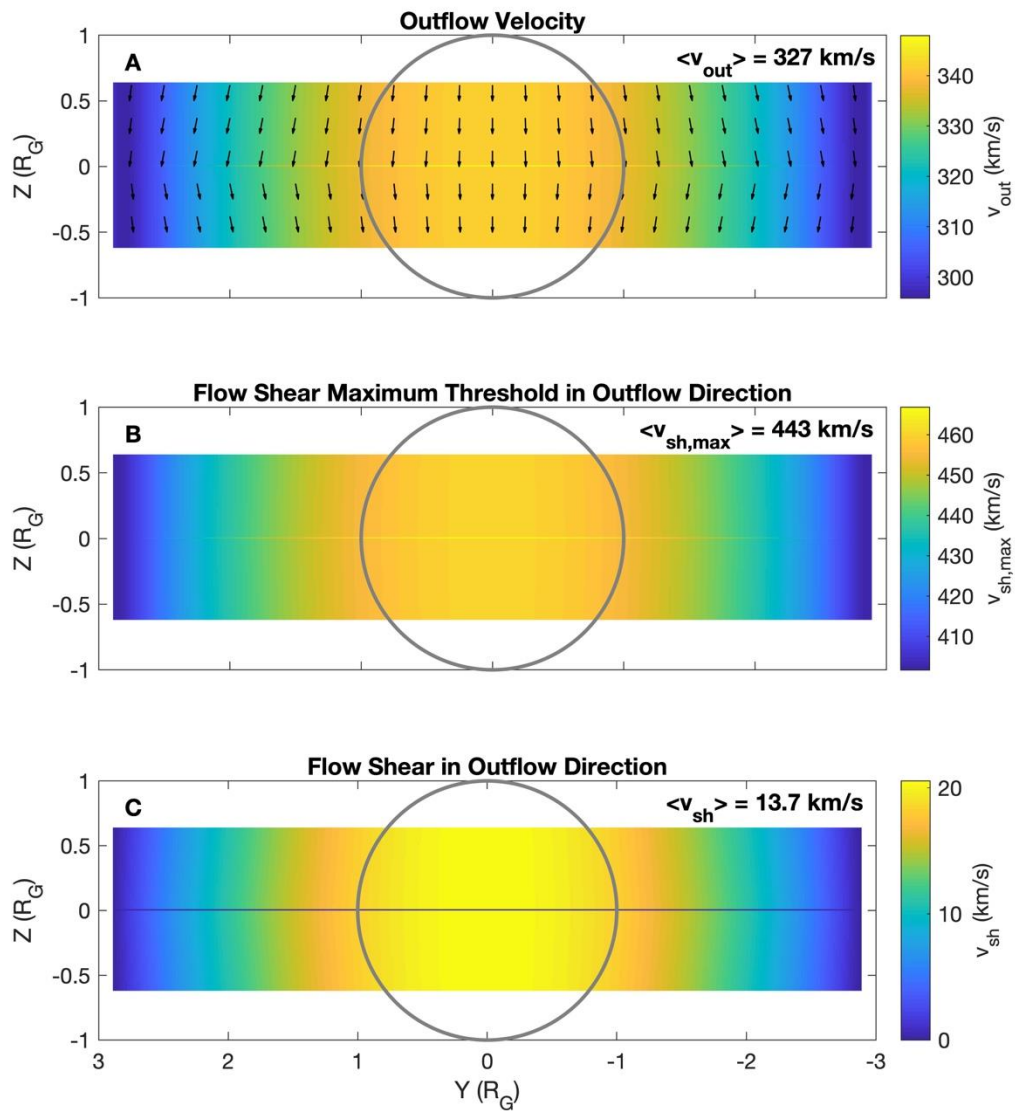
521

522 Figure 1: Magnetopause conditions projected onto a two-dimensional plane with the Jovian
 523 plasma flowing into the page when Ganymede is in the Jovian current sheet. Parameters shown
 524 are (A) X-coordinates on the magnetopause surface, (B) Jovian-side mass density, (C) Jovian-
 525 side plasma pressure, (D) Jovian-side flow velocity, (E) Jovian-side magnetic field, and (F)
 526 Ganymede-side magnetic field. Ganymede is outlined in grey and the closed-field region is
 527 defined between two red dashed lines.



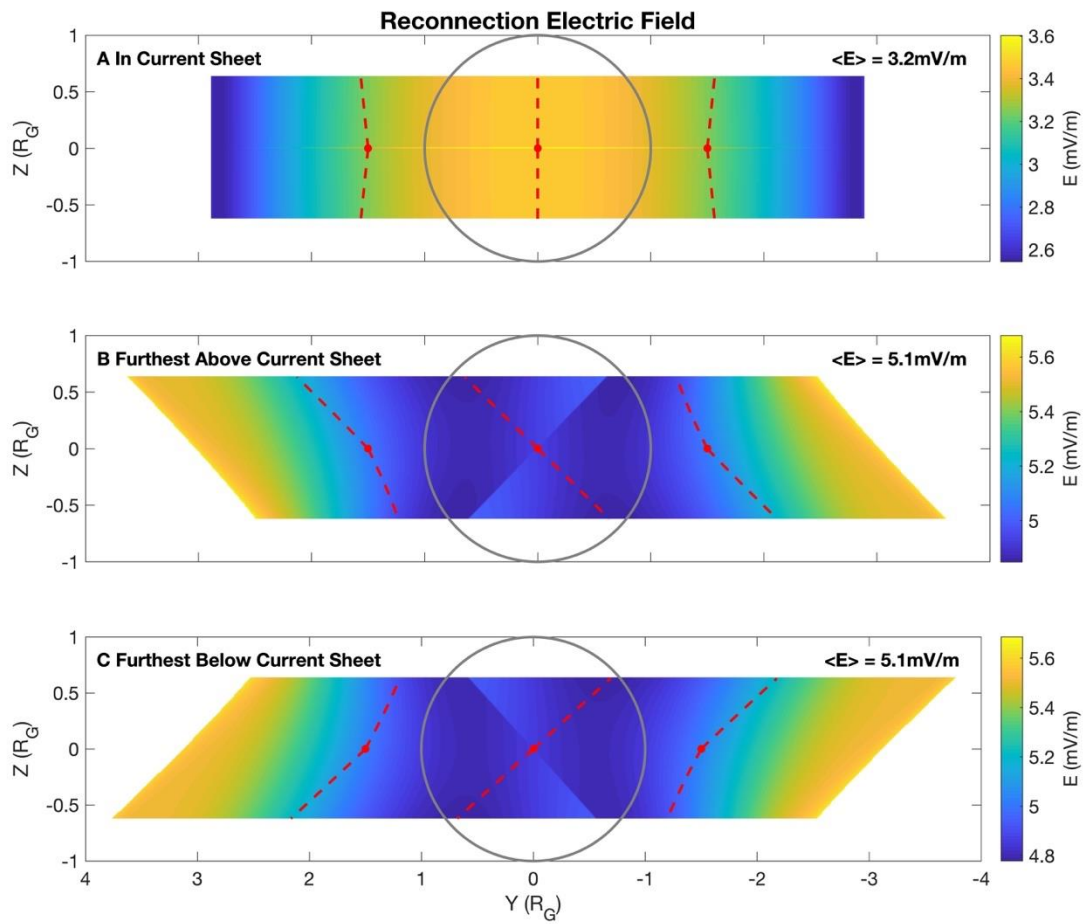
528

529 Figure 2: Evaluation of the diamagnetic drift onset condition in Ganymede's closed-field
 530 region when Ganymede is in the Jovian current sheet. Parameters shown are (A) beta difference
 531 across the magnetopause, (B) magnetic shear angle minimum threshold, and (C) shear angle
 532 calculated from magnetopause conditions. Ganymede is outlined in grey and average parameter
 533 values are shown at top right.



534

535 Figure 3: Evaluation of the bulk plasma flow shear onset condition in Ganymede's closed-field
 536 regions when Ganymede is in the Jovian current sheet. Parameters shown are (A) reconnection
 537 outflow velocity, (B) flow shear maximum threshold, and (C) flow shear calculated from
 538 magnetopause conditions. The format is the same as Figure 2.



539

540 Figure 4: Electric field at potential reconnection sites in Ganymede's closed-field regions
 541 computed when Ganymede is (A) in, (B) furthest above, and (C) furthest below the Jovian
 542 current sheet. Red dashed lines indicate plasma outflow tracks from selected reconnection sites.
 543 The format is the same as Figure 2.